MIMO Capacity Enhancement Using Parasitic Reconfigurable Aperture Antennas (RECAPs)

Rashid Mehmood, *Student Member, IEEE*, and Jon W. Wallace, *Member, IEEE*

***Abstract*—The capacity of multiple-input multiple-output (MIMO) systems employing reconfigurable apertures (RECAPs) is carefully analyzed with a realistic thermal noise model for three different power constraints: average receive signal-to-noise ratio (SNR), maximum effective isotropic radiated power (EIRP), and average transmit power. Performance is studied not only for a noise-limited single link, but also in the presence of interference and multiple RECAP-equipped users. The impact of loss and finite bandwidth on the operation of the RECAP is also considered. For the practical EIRP constraint, results show that a compact MIMO RECAP ($1\lambda \times 1\lambda$) provides 30%–50% capacity improvement for a single link. It is also found that RECAPs are even more beneficial in interference-limited and multiuser scenarios, where capacity is increased by 50% to 800% depending on the severity of the interference, indicating that RECAPs are an attractive solution for future wireless systems employing aggressive spectral reuse.**

***Index Terms*—Information rates, interference suppression, multiple-input multiple-output (MIMO) systems, reconfigurable antennas.**

I. Introduction

RELIABLE and high performance transmission continues to be a major goal of wireless communication systems, which is significantly enhanced by arrays employing beamforming and diversity techniques. Multiple-input multiple-output (MIMO) wireless technology emerged in the 1980s and has gained increasing attention due to the significant gains in channel capacity [1], [2], possible by exploiting channel multi-path with spatial multiplexing. In a communication system, the channel matrix includes effects of the physical propagation environment and antenna radiation and reception characteristics. Antennas can be viewed as transmit and receive filters that are ideally matched to the physical channel, enhancing signals of interest and mitigating noise and interference to maximize capacity [3]. Although for a single fixed antenna, no adaptation of spatial filtering is possible, multiple fixed antennas connected to multiple radio frequency (RF) and digital signal processing (DSP) chains can employ the "smart antenna" concept [4] to provide dynamic spatial filtering. However, the increased RF and DSP resources may be prohibitive for many applications.

The term reconfigurable aperture (RECAP) antenna [5], [6] refers to a large array of analog reconfigurable elements (REs), which can be manipulated in order to support beam-steering, signal-to-noise (SNR) maximization, interference suppression, and dynamic matching. In contrast to smart antennas, RECAPs adapt directly in the analog radio-frequency (RF) domain and require only a single RF chain and modest DSP resources, potentially providing lower cost. RECAPs are also interesting for MIMO systems, where the optimal antenna array exploits the multi-path to provide peak capacity while using as few active RF chains as possible. Also, for multi-user systems RECAPs can adapt patterns to dynamically partition spatial reuse of spectral resources.

Optimal antenna selection for MIMO has been considered (e.g., [7]), where only a few antennas out of a set of antennas are chosen for capacity maximization with lower complexity. The improvement in the channel capacity using a reconfigurable antenna is presented in [8], where moderate sized switched parasitic arrays with relatively few REs are used. A practical antenna solution providing multiple patterns with a single fixed antenna is presented in [9], exhibiting improved performance compared to spatially separated dipoles. Capacity maximization using planar RECAPs at transmit and receive is investigated in [10], where each antenna acts as a single RECAP. A reconfigurable MIMO array consisting of two dipole elements is introduced in [11], where by adaptively changing the length of the dipoles, modest increases in single-user capacity are possible. The important study in [12] shows that MIMO systems with reconfigurable antennas have a maximum diversity order equal to the product of the number of transmit antennas, receive antennas, and the reconfigurable states. This idea is expanded in [13], where not only practical space-time coding methods that code over the antenna state to maximize diversity are developed, but also practical aspects like antenna switching time are considered.

This previous work on reconfigurable MIMO systems has some limitations. First, only simple termination-independent receiver noise has been considered, which is known to be inaccurate for analyzing MIMO systems with variable termination [14]. Second, limited reconfigurability has been considered, which may be insufficient to exploit the degrees of freedom of the occupied aperture. Third, the role of the power constraint has not been studied in detail, where typically only an average transmit power constraint has been assumed. Finally, capacity maximization for a single link limited by thermal noise has been

Manuscript received July 21, 2010; revised November 30, 2010; accepted January 15, 2011. Date of publication October 25, 2011; date of current version February 03, 2012.

The authors are with the School of Engineering and Science, Jacobs University Bremen, Bremen 28759, Germany (e-mail: r.mehmood@ieee.org; wall@ieee.org).

Color versions of one or more of the figures in this paper are available online at http://ieeexplore.ieee.org.

Digital Object Identifier 10.1109/TAP.2011.2173445

considered, but multi-user systems with interference are more realistic for today's wireless scenarios.

This work provides a more comprehensive analysis of capacity enhancement possible with reconfigurable antennas by addressing these previous shortcomings. To this end, we study a RECAP consisting of a 9×9 parasitic array having sufficient complexity to exploit a compact $1\lambda \times 1\lambda$ aperture as studied in [15]. In contrast to [10], the complete aperture is exploited rather than using separate RECAPs for each MIMO antenna. A realistic noise model is considered in order to take into account the effect of matching on amplifier noise. Three realistic but distinct power constraints are also considered, indicating where RECAPs are most effective: 1) average signal-to-noise (SNR), where transmit and receive power are normalized and the focus of optimization is on channel orthogonality and multi-path enhancement; 2) effective isotropic radiated power (EIRP), which allows power enhancement at receiver but not at transmitter, which is more practical for many of today's communication systems; and 3) average transmit power, which is a commonly assumed constraint allowing power enhancement at both transmit and receive. In addition to considering a single link limited by thermal noise, we also consider fixed interference and multiple RECAP-equipped links.

The remainder of the paper is organized as follows: Section II explains the simulation method that was used to study RECAPs, followed by Section III that defines MIMO capacity with power constraints. Section IV studies the MIMO channel capacity using RECAP antennas in comparison with non-RECAP arrays, and Section V concludes the paper.

II. Analysis of Parasitic RECAP Structure

The structure considered in this study is depicted in Fig. 1(a), which is a 9×9 dipole array consisting of z-oriented half-wave dipoles constrained to an area of $1\lambda \times 1\lambda$ in the xy plane. Each dipole is either an active "feed" (connected to a transmit or a receive chain) or terminated with a reconfigurable element (RE), each of which has 8 possible reconfigurable states (RSs) to ensure sufficient control over the aperture [15]. The top view of the structure is shown in Fig. 1(b), where REs and feeds are indicated by squares and circles, respectively. In this work, we consider propagation in the xy plane, where the two-dimensional array can generate patterns with both endfire and broadside characteristics.

REs are assumed to be variable capacitances, such that the reflection coefficient presented at the kth port is $\Gamma_k = e^{j\alpha_k}$, where $\alpha_k \in [-180°, 0°]$. We have assumed that α_k is uniformly distributed on $[-180°, 0°]$ as presented in [15]. Although planar RECAPs with realistic RE biasing are arguably more practical, this study employs this simple structure, since it can be simulated efficiently and its performance is not constrained by practical limitations of existing switch technologies, biasing, substrate losses, etc.

Time required for RE switching for a dynamic reconfigurable antenna was treated in [13] for MEMS switches, indicating that this overhead can significantly impact system throughput. For our analyzed structure employing variable capacitances (i.e. varactor diodes), the switching time is expected to be a few ns, which is on the order of a symbol for existing modulation standards. Thus, switching at the beginning of a transmission frame should incur negligible overhead. On the other hand, if tunable MEMS devices are used, switching times could be higher, requiring longer block lengths to mitigate overhead as explained in [13]. Although a detailed analysis of switching time for dynamic adaption in time-varying channels is beyond the scope of this paper, this remains an important consideration for practical systems. Thus, this present work demonstrates the benefit of the RECAP concept for MIMO systems, and practical aspects are to be treated in future work.

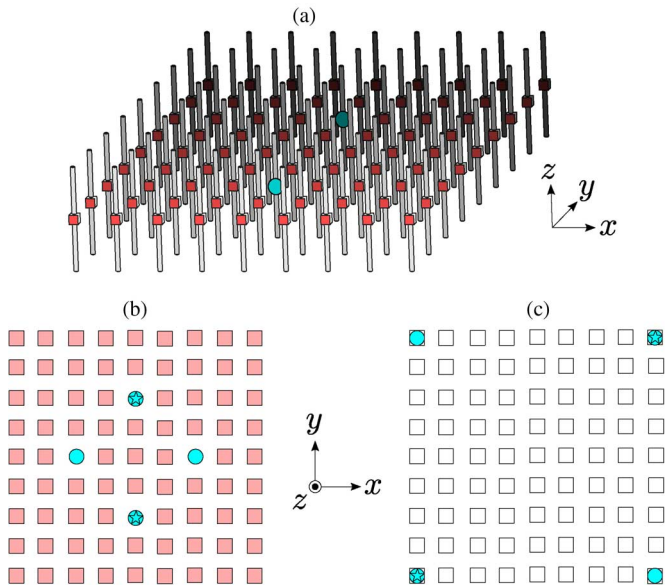

Fig. 1. Configurations for non-RECAP and RECAP arrays: (a) perspective view of the parasitic RECAP with 2 feeds. (b) Top view of RECAP configurations, where red boxes show RE positions, blue stars and circles show feed locations for 2×2 and 4×4 MIMO respectively. (c) Top view of antenna positions for non-RECAP for 2×2 MIMO (stars) and 4×4 MIMO (circles), where boxes are empty locations.

A. Efficient Simulation of RECAP Structure

Efficient simulation of the RECAP is accomplished by combining full-wave simulation of the array with network analysis for RE loading. The structure is first analyzed using the Numerical Electromagnetics Code (NEC), which yields the admittance matrix $\mathbf{Y}$ and short circuit embedded radiation patterns $\mathbf{E}^{\mathrm{sc}}(\theta, \phi)$ of the arrays, where $e^{\mathrm{sc}}_{pk}(\theta, \phi)$ gives the radiation into polarization p for unit voltage excitation on port k, when the other ports are short-circuited. S-parameter analysis is more convenient for this study, where the S-parameter matrix $\mathbf{S}$ and matched (Z_0-terminated) patterns $\mathbf{E}^{\mathrm{mc}}$ are computed as

$$\mathbf{S} = (\mathbf{I} + Z_0\mathbf{Y})^{-1}(\mathbf{I} - Z_0\mathbf{Y}) \tag{1}$$

and

$$\mathbf{E}^{\mathrm{mc}}(\theta, \phi) = \frac{\mathbf{E}^{\mathrm{sc}}(\theta, \phi)}{\sqrt{Z_0}}\mathbf{Z}(\mathbf{I} - \mathbf{S}) \tag{2}$$

respectively, where Z_0 is the real scalar normalizing impedance, and $\mathbf{I}$ is the identity matrix. Note that the matched circuit patterns in (2) are embedded patterns, where the entry $e^{\mathrm{mc}}_{pk}(\theta, \phi)$ gives the pattern radiated into polarization p when port k is

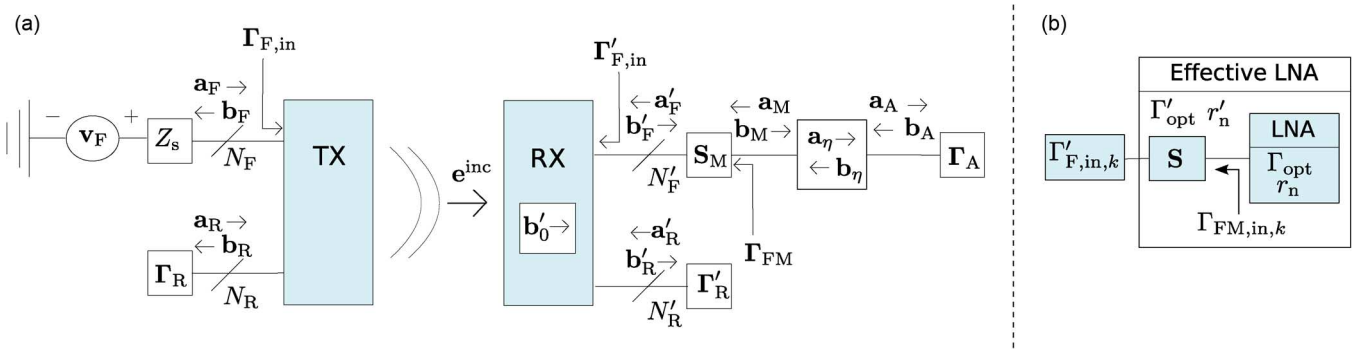

Fig. 2. MIMO system model and noise matching for LNAs. (a) System model; (b) LNA matching.

driven with a unit incident wave and the other ports are terminated in Z_0 loads ($\Gamma = 0$).

Next, network analysis is used to find radiation patterns and the input reflection matrix of the feeds for arbitrary RE termination. Defining $\mathbf{a}_{\mathrm{F}}$ and $\mathbf{b}_{\mathrm{F}}$ as the $N_{\mathrm{F}} \times 1$ vectors of incident and reflected waves on the feed ports and $\mathbf{a}_{\mathrm{R}}$ and $\mathbf{b}_{\mathrm{R}}$ as the corresponding $N_{\mathrm{R}} \times 1$ vectors on the RE ports

$$\underbrace{\begin{bmatrix}\mathbf{b}_{\mathrm{F}}\\ \mathbf{b}_{\mathrm{R}}\end{bmatrix}}_{\mathbf{b}} = \underbrace{\begin{bmatrix}\mathbf{S}_{\mathrm{FF}} & \mathbf{S}_{\mathrm{FR}}\\ \mathbf{S}_{\mathrm{RF}} & \mathbf{S}_{\mathrm{RR}}\end{bmatrix}}_{\mathbf{S}} \underbrace{\begin{bmatrix}\mathbf{a}_{\mathrm{F}}\\ \mathbf{a}_{\mathrm{R}}\end{bmatrix}}_{\mathbf{a}} \tag{3}$$

where $\mathbf{S}$ has been partitioned according to feeds and REs. Terminating RE ports with loads having reflection matrix $\mathbf{\Gamma}_{\mathrm{R}}$, we have $\mathbf{a}_{\mathrm{R}} = \mathbf{\Gamma}_{\mathrm{R}}\mathbf{b}_{\mathrm{R}}$, where $\mathbf{\Gamma}_{\mathrm{R}}$ is a diagonal matrix with $\Gamma_{\mathrm{R},kk} = \Gamma_{\mathrm{R},k}$. Combined with (3)

$$\mathbf{a}_R = \mathbf{\Gamma}_{\mathrm{R}}(\mathbf{I} - \mathbf{S}_{\mathrm{RR}}\mathbf{\Gamma}_{\mathrm{R}})^{-1}\mathbf{S}_{\mathrm{RF}}\mathbf{a}_{\mathrm{F}} \tag{4}$$

$$\mathbf{b}_{\mathrm{F}} = \underbrace{\left[\mathbf{S}_{\mathrm{FF}} + \mathbf{S}_{\mathrm{FR}}\mathbf{\Gamma}_{\mathrm{R}}(\mathbf{I} - \mathbf{S}_{\mathrm{RR}}\mathbf{\Gamma}_{\mathrm{R}})^{-1}\mathbf{S}_{\mathrm{RF}}\right]}_{\mathbf{\Gamma}_{\mathrm{F,in}}}\mathbf{a}_{\mathrm{F}} \tag{5}$$

where $\mathbf{\Gamma}_{\mathrm{F,in}}$ is the input reflection coefficient matrix looking into the feed ports for the given termination at the REs. In this work, we choose $Z_0 = 72\ \Omega$ to be closely matched to a single half-wave dipole. The field radiation pattern of the RECAP with RE termination is

$$\mathbf{e}(\theta,\phi) = \underbrace{\left[\mathbf{E}^{\mathrm{mc}}_{\mathrm{F}}(\theta,\phi) \quad \mathbf{E}^{\mathrm{mc}}_{\mathrm{R}}(\theta,\phi)\right]}_{\mathbf{E}^{\mathrm{mc}}(\theta,\phi)}\begin{bmatrix}\mathbf{a}_{\mathrm{F}}\\ \mathbf{a}_{\mathrm{R}}\end{bmatrix} \tag{6}$$

where $\mathbf{E}^{\mathrm{mc}}_{\mathrm{F}}(\theta,\phi)$ and $\mathbf{E}^{\mathrm{mc}}_{\mathrm{R}}(\theta,\phi)$ represent matched patterns corresponding to feeds and REs respectively. Substituting (4) into (6) yields

$$\mathbf{e}(\theta,\phi) = \underbrace{\left[\mathbf{E}^{\mathrm{mc}}_{\mathrm{F}}(\theta,\phi) + \mathbf{E}^{\mathrm{mc}}_{\mathrm{R}}(\theta,\phi)\mathbf{\Gamma}_{\mathrm{R}}(\mathbf{I} - \mathbf{S}_{\mathrm{RR}}\mathbf{\Gamma}_{\mathrm{R}})^{-1}\mathbf{S}_{\mathrm{RF}}\right]}_{\mathbf{E}^{\mathrm{mc}}_{\mathrm{FT}}(\theta,\phi)}\mathbf{a}_{\mathrm{F}} \tag{7}$$

where $\mathbf{E}^{\mathrm{mc}}_{\mathrm{FT}}(\theta,\phi)$ represents matched patterns of feed ports with RE port termination $\mathbf{\Gamma}_{\mathrm{R}}$.

B. System Model

Next, we consider using RECAPs at transmitter (Tx) and receiver (Rx) to form a complete system, as depicted in Fig. 2(a). Note that unprimed and primed RECAP quantities denote those at Tx and Rx, respectively. At Tx the kth feed is connected to source voltage $\mathrm{v}_{\mathrm{F},k}$ with internal impedance $Z_s = Z_0$. The incident traveling waves $\mathbf{a}_{\mathrm{F}}$ on the feed ports are simply $\mathbf{a}_{\mathrm{F}} = \mathbf{v}_{\mathrm{F}}/(2\sqrt{Z_0})$, and radiated far fields are given by (7). The RE-terminated receive array is modeled in a similar manner, expect that due to external incident field, a source wave term $\mathbf{b}'_0$ must be included, such that $\mathbf{b}'_{\mathrm{F}} = \mathbf{\Gamma}'_{\mathrm{F,in}}\mathbf{a}'_{\mathrm{F}} + \mathbf{b}'_0$. Assuming a plane wave arriving at angle $(\theta'_\ell, \phi'_\ell)$ and reciprocity

$$\mathbf{b}'_0 = \left[\mathbf{E}^{\mathrm{mc}'}_{\mathrm{FT}}(\theta'_\ell,\phi'_\ell)\right]^{\mathrm{T}}\mathbf{e}^{\mathrm{inc}}(\theta'_\ell,\phi'_\ell) \tag{8}$$

where $\mathbf{e}^{\mathrm{inc}}$ gives the polarization and complex amplitude of the plane wave.

A multi-path model is assumed consisting of K clusters and L_k paths (or rays) within the kth cluster, where the ℓth path in the kth cluster has angle of departure $(\theta_{k\ell}, \phi_{k\ell})$, angle of arrival $(\theta'_{k\ell}, \phi'_{k\ell})$, complex amplitude $\alpha_{k\ell}$, and time of arrival $\tau_{k\ell}$, or $\mathbf{e}^{\mathrm{inc}}(\theta'_{k\ell}, \phi'_{k\ell}) = \alpha_{k\ell}e^{-j\omega\tau_{k\ell}}\mathbf{e}(\theta_{k\ell}, \phi_{k\ell})$, where ω is frequency. Although depolarization of the paths is not considered in this work, this could be included by making $\alpha_{k\ell}$ a matrix. Superimposing the waves due to all paths

$$\mathbf{b}'_0 = \underbrace{\sum_{k=1}^{K}\sum_{\ell=1}^{L_k}\left[\mathbf{E}^{\mathrm{mc}'}_{\mathrm{FT}}(\theta'_{k\ell},\phi'_{k\ell})\right]^{T}\alpha_{k\ell}e^{-j\omega\tau_{k\ell}}\mathbf{E}^{\mathrm{mc}}_{\mathrm{FT}}(\theta_{k\ell},\phi_{k\ell})}_{\mathbf{S}_{\mathrm{Rx,Tx}}}\mathbf{a}_{\mathrm{F}}. \tag{9}$$

C. Noise Modeling

In order to consider a realistic system, where noise from the low-noise amplifier (LNA) at the receiver depends on the feed reflection, we employ an LNA model equivalent to [14], where equivalent forward ($\mathbf{a}_\eta$) and reverse ($\mathbf{b}_\eta$) traveling noise waves at the LNA input are needed to properly model real transistors. The receiver consists of a matching network, forward and reverse noise sources, and LNA as shown in Fig. 2(a). The multiport LNA is assumed to consist of multiple uncoupled LNAs with optimal reflection coefficient Γ_{opt}, normalized equivalent noise resistance r_n, and minimum noise figure F_{min}, available from a standard LNA data sheet.

Straightforward analysis at the connection of array and matching network reveals

$$\mathbf{b}_{\mathrm{M}} = \mathbf{\Gamma}_{\mathrm{FM}}\mathbf{a}_{\mathrm{M}} + \mathbf{b}_{\mathrm{FM}} \tag{10}$$

where

$$\mathbf{\Gamma}_{\mathrm{FM}} = \mathbf{S}_{\mathrm{M},22} + \mathbf{S}_{\mathrm{M},21}\mathbf{\Gamma}'_{\mathrm{F,in}}\left(\mathbf{I} - \mathbf{S}_{\mathrm{M},11}\mathbf{\Gamma}'_{\mathrm{F,in}}\right)^{-1}\mathbf{S}_{\mathrm{M},12} \quad (11)$$

$$\mathbf{b}_{\mathrm{FM}} = \mathbf{S}_{\mathrm{M},21}\left[\mathbf{I} + \mathbf{\Gamma}'_{\mathrm{F,in}}\left(\mathbf{I} - \mathbf{S}_{\mathrm{M},11}\mathbf{\Gamma}'_{\mathrm{F,in}}\right)^{-1}\mathbf{S}_{\mathrm{M},11}\right]\mathbf{b}'_o. \quad (12)$$

The incident wave $\mathbf{a}_{\mathrm{A}}$ into the amplifier is found to be,

$$\mathbf{a}_{\mathrm{A}} = \underbrace{[\mathbf{I} - \mathbf{\Gamma}_{\mathrm{FM}}\mathbf{\Gamma}_A]^{-1}}_{\mathbf{Q}}(\mathbf{\Gamma}_{\mathrm{FM}}\mathbf{b}_\eta + \mathbf{a}_\eta + \mathbf{b}_{\mathrm{FM}}). \quad (13)$$

In this work, a fixed (non-RECAP) array is used as a reference case for gauging performance improvement, and an identical uncoupled matching network is assumed on each of the N'_{F} receive feeds such that $\mathbf{\Gamma}_{\mathrm{FM}} \approx \Gamma_{\mathrm{opt}}\mathbf{I}$ for the reference, where Γ_{opt} is the source reflection coefficient that provides optimal noise performance. The same uncoupled matching network is employed for the RECAP, and noise coupling from one feed to the next and deviation of $\mathbf{\Gamma}_{\mathrm{FM}}$ can lead to reduced SNR.

Fig. 2(b) shows the uncoupled matching arrangement on each branch that transforms $\Gamma'_{\mathrm{F,in},k} = 0$ to $\Gamma_{\mathrm{FM,in},k} = \Gamma_{\mathrm{opt}}$ using a reciprocal lossless matching network, such that $\mathbf{S}^H\mathbf{S} = \mathbf{I}$, where $\mathbf{S}$ is a 2×2 matrix. The required conditions are satisfied with

$$S_{11} = S_{22} = \Gamma_{\mathrm{opt}} \quad (14)$$

$$S_{12} = S_{21} = j\sqrt{1 - |\Gamma_{\mathrm{opt}}|^2}e^{j\angle\Gamma_{\mathrm{opt}}}. \quad (15)$$

$\mathbf{S}_{\mathrm{M}}$ is a 2×2 block matrix, where the ijth block is equal to $S_{ij}\mathbf{I}$ from (14) and (15), and $\mathbf{I}$ is an $N'_{\mathrm{F}} \times N'_{\mathrm{F}}$ identity matrix. Note that the fixed matching network can also be lumped into the LNA to form the effective LNA shown in Fig. 2(b), with new optimal reflection coefficient Γ'_{opt} and equivalent noise resistance r'_{n}.

Plugging (9) into (12) and the result into (13) yields

$$\underbrace{\mathbf{a}_{\mathrm{A}}}_{\mathbf{y}} = \mathbf{Q}\Big(\underbrace{\Gamma_{FM}\mathbf{b}_\eta + \mathbf{a}_\eta}_{\mathbf{n}} + \underbrace{\mathbf{S}_{\mathrm{M},21}\Big[\mathbf{I} + \mathbf{\Gamma}'_{\mathrm{F,in}}\left(\mathbf{I} - \mathbf{S}_{\mathrm{M},11}\mathbf{\Gamma}'_{\mathrm{F,in}}\right)^{-1}\mathbf{S}_{\mathrm{M},11}\Big]\mathbf{S}_{\mathrm{Rx,Tx}}}_{\mathbf{H}}\underbrace{\mathbf{a}_{\mathrm{F}}}_{\mathbf{x}}\Big) \quad (16)$$

where $\mathbf{H}$ is the channel matrix, $\mathbf{S}_{\mathrm{Rx,Tx}}$ is from (9), $\mathbf{n}$ is noise, and $\mathbf{x}$ and $\mathbf{y}$ are input and output signals. The linear term $\mathbf{Q}$ applied to both signal and noise does not change capacity and is omitted. The noise covariance $\mathbf{R}_\eta = \mathbf{E}\{\mathbf{n}\mathbf{n}^H\}$ is

$$\mathbf{R}_\eta = \mathbf{\Gamma}_{\mathrm{FM}}\mathbf{\Gamma}^H_{\mathrm{FM}}\sigma^2_{\mathrm{b}} + \mathbf{I}\sigma^2_{\mathrm{a}} + 2\mathrm{Re}\{\mathbf{\Gamma}_{\mathrm{FM}}\sigma_{\mathrm{ba}}\} \quad (17)$$

where σ^2_{b}, σ^2_{a}, and σ_{ba} are [16]

$$\sigma^2_{\mathrm{b}} = \mathbf{E}\{|b_{\eta,i}|^2\} = \frac{\sigma^2_{\mathrm{v}}}{Z_0}\left[-\frac{F_{\min}-1}{4r_{\mathrm{n}}} + \frac{1}{|1+\Gamma_{\mathrm{opt}}|^2}\right] \quad (18)$$

$$\sigma^2_{\mathrm{a}} = \mathbf{E}\{|a_{\eta,i}|^2\} = \frac{\sigma^2_{\mathrm{v}}}{Z_0}\left[\frac{F_{\min}-1}{4r_{\mathrm{n}}} + \frac{|\Gamma_{\mathrm{opt}}|^2}{|1+\Gamma_{\mathrm{opt}}|^2}\right] \quad (19)$$

$$\sigma_{\mathrm{ba}} = \mathbf{E}\{b_{\eta,i}a^*_{\eta,i}\} = \frac{\sigma^2_{\mathrm{v}}}{Z_0}\frac{|\Gamma_{\mathrm{opt}}|}{|1+\Gamma_{\mathrm{opt}}|^2}e^{j(\pi - \angle\Gamma_{opt})} \quad (20)$$

where $r_{\mathrm{n}} = R_{\mathrm{n}}/Z_0$, R_{n} is the equivalent-noise resistance, $\sigma^2_{\mathrm{v}} = 4P_{\mathrm{ref}}R_{\mathrm{n}}$ is the noise voltage covariance, $P_{\mathrm{ref}} = \kappa T_0 W$, κ is Bolzmann's constant, T_0 is reference temperature, and W is bandwidth. Since P_{ref} is the same for the reference and RECAP systems and SNR of the reference system is fixed, P_{ref} has no effect on capacity and is set to 1.

Note that since a data sheet typically assumes $Z_0 = 50\ \Omega$, which is different from the value used in our analysis, the transformation

$$\Gamma_{\mathrm{opt}} = \frac{Z^{\mathrm{ds}}_0\left(1 + \Gamma^{\mathrm{ds}}_{\mathrm{opt}}\right) - Z_0\left(1 - \Gamma^{\mathrm{ds}}_{\mathrm{opt}}\right)}{Z^{\mathrm{ds}}_0\left(1 + \Gamma^{\mathrm{ds}}_{\mathrm{opt}}\right) + Z_0\left(1 - \Gamma^{\mathrm{ds}}_{\mathrm{opt}}\right)} \quad (21)$$

is required, where $\Gamma^{\mathrm{ds}}_{\mathrm{opt}}$ and Z^{ds}_0 are optimal reflection and reference impedance from the data sheet.

Summarizing, the MIMO input-output relationship is given by (16), where RE-dependent noise covariance $\mathbf{R}_\eta$ is computed from (17)–(20), where parameters R_{n}, $\Gamma^{\mathrm{ds}}_{\mathrm{opt}}$, and $F_{\min}$ are available from a standard LNA specification. Although computation of the noise covariance in this way seems cumbersome compared to MIMO analyses that directly specify $\mathbf{R}_\eta$, the added complexity is necessary to capture noise coupling of the active ports and variable input impedance of the receive array, which both affect capacity when thermal noise is significant compared to interference.

D. LNA Specification

This analysis uses the MAXIM MAX2656 LNA, having $F_{\min} = 1.79$ dB, noise-equivalent resistance $R_{\mathrm{n}} = 43.23\ \Omega$, and optimum reflection coefficient $\Gamma^{\mathrm{ds}}_{\mathrm{opt}} = 0.130\angle 124.5°$ (at 1960 MHz and $Z^{\mathrm{ds}}_0 = 50\ \Omega$) [17]. Since the specific LNA may affect the simulations and conclusions, we briefly consider the impact of the LNA choice.

Analysis of the RECAP mainly depends on how sensitive the noise figure of the LNA is to the reflection coefficient presented by the RECAP. Noise figure for uncoupled LNAs is [16]

$$F = F_{\min} + 4r_{\mathrm{n}}\frac{|\Gamma_{\mathrm{in}} - \Gamma_{\mathrm{opt}}|^2}{|1+\Gamma_{\mathrm{opt}}|^2\left(1 - |\Gamma_{\mathrm{in}}|^2\right)} \quad (22)$$

where Γ_{in} is the reflection coefficient looking into the output of one of the matching networks. Assuming a lossless matching network shown in Fig. 2(b) that transforms the source reflection $\Gamma'_{\mathrm{F,in},k} = 0$ to $\Gamma_{\mathrm{FM,in},k} = \Gamma_{\mathrm{opt}}$ of the LNA, it can be shown that for $\Gamma'_{\mathrm{F,in},k} \neq 0$,

$$F = F_{\min} + 4\underbrace{r_{\mathrm{n}}\frac{1 - |\Gamma_{\mathrm{opt}}|^2}{|1+\Gamma_{\mathrm{opt}}|^2}}_{r'_{\mathrm{n}}}\frac{\left|\Gamma'_{\mathrm{F,in},k}\right|^2}{1 - \left|\Gamma'_{\mathrm{F,in},k}\right|^2} \quad (23)$$

where r'_{n} is the the equivalent LNA noise resistance referenced back to the input of the matching network where $\Gamma'_{\mathrm{opt}} = 0$.

Fig. 3 shows noise figure degradation $F - F_{\min}$ in dB for different values of r'_n and $|\Gamma_{\mathrm{in}}|^2$ using (23), where $\Gamma_{\mathrm{in}} \triangleq \Gamma_{\mathrm{F,in},k}$. As r'_n increases, the penalty of mismatch can increase dramatically. However, our chosen amplifier (as indicated in the figure) has moderate sensitivity to mismatch, making it a good candidate for this initial study. Amplifiers with much higher r'_n would

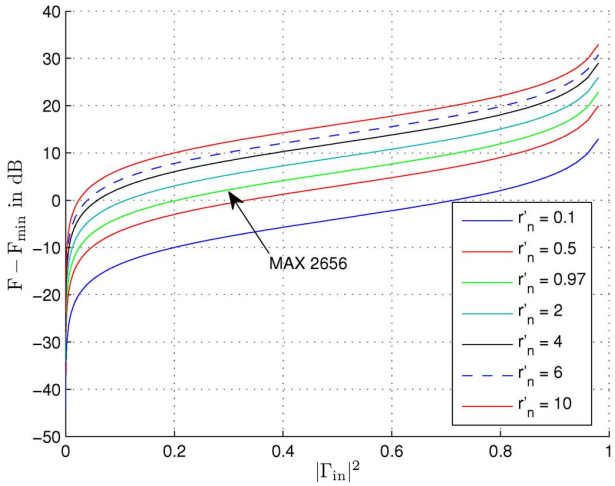

Fig. 3. Effects of $r'_{\rm n}$ and $|\Gamma_{\rm in}|^2$ on $F - F_{\rm min}$.

simply increase mismatch penalty, which would more strongly constrain the set of useful RECAP states, possibly resulting in reduced capacity.

E. MIMO Channel Modeling

The channel matrix $\mathbf{H}$ is given by (16), where $\mathbf{S}_{\rm Rx,Tx}$ is found according to the path-based model in (9). In this work we consider models where attention is restricted to the azimuthal plane (θ and θ' are 90°). Two propagation models are assumed for the paths between Tx and Rx:

1) Uniform Model: In this simple model, a single cluster is assumed ($K = 1$) with $L = L_1$ rays having arrival times $\tau_{1\ell} = 0$. Angles of arrival ($\phi'_{1\ell}$) and departure ($\phi_{1\ell}$) are uniformly distributed on $[0°, 360°]$ and $\alpha_{1\ell}$ has a unit variance complex normal distribution.

2) SVA Model: The more realistic Saleh-Valenzuela angular (SVA) model [18] assumes K clusters, where the arrival of the kth cluster (τ_k) has the conditional pdf

$$p(\tau_k|\tau_{k-1}) = \Lambda e^{-\Lambda(\tau_k - \tau_{k-1})}, \quad \tau_{k-1} < \tau_k < \infty, \quad \tau_1 = 0 \tag{24}$$

where Λ is the arrival rate of the clusters. Relative arrival time of the ℓth ray within the kth cluster has the pdf

$$p(\tau_{k\ell}|\tau_{k,\ell-1}) = \lambda e^{-\lambda(\tau_{k\ell} - \tau_{k,\ell-1})}, \tau_{k,\ell-1} < \tau_{k\ell} < \infty, \tau_{k1} = \tau_k \tag{25}$$

where λ is the arrival rate of rays.

The complex amplitude of the ℓth ray in the kth cluster ($\alpha_{k\ell}$) is complex gaussian, where the variance decays exponentially with arrival time according to

$$\mathbf{E}\left\{|\alpha_{k\ell}|^2\right\} = e^{-\tau_k/T_C} e^{-(\tau_{k\ell} - \tau_k)/T_R} \tag{26}$$

and T_C and T_R are the cluster and ray decay time constant, respectively. The azimuthal angle of the kth cluster at transmit and receive is Φ_k and Φ'_k, respectively, which are uniformly distributed on $[0°, 360°]$. The relative transmit and receive angles of the ℓth ray in the kth cluster are $\nu_{k\ell} = \phi_{k\ell} - \Phi_k$ and $\nu'_{k\ell} = \phi'_{k\ell} - \Phi'_k$, which follow a double-sided Laplacian distribution with pdf $p(\nu) = 1/(\sqrt{2}\sigma)\exp[-|\sqrt{2}\nu/\sigma|]$, where σ is the angular spread.

Although RECAPs that can adapt to each instantaneous value of $\alpha_{k\ell}$, $\phi_{k\ell}$ and $\phi'_{k\ell}$ are optimal, this rate of adaptation may be unrealistic for practical implementation. Thus we also consider a system that adapts average RECAP performance when the $\phi_{k\ell}$ and $\phi'_{k\ell}$ are fixed, but only the $\alpha_{k\ell}$ are random. We refer to the former and latter cases as instantaneous and average RECAP optimization, where average performance is computed in the latter case using 10 realizations of $\alpha_{k\ell}$.

F. Genetic Algorithm

Due to the large number of RE combinations, obtaining the optimal solution with an exhaustive search is not feasible, and a genetic algorithm (GA) is employed. The GA employed in this work is basically equivalent to that described in [15], except that REs at both transmit and receive end are jointly optimized to maximize the capacity.

Note that the purpose of using genetic algorithms in this work is only to explore the peak potential of RECAP-enabled MIMO, since such algorithms may be too expensive for in-situ optimization due to the extensive training overhead and computation time required. The development of direct RECAP optimization methods more suitable for real-time optimization is a long-term goal of this research, to be treated in later work.

III. MIMO Capacity With Constraints

For the analysis of MIMO channel capacity, we have used the RECAP structure explained in Section II, for both Tx and Rx, forming a MIMO system. In order to properly scale power and assess RECAP capacity gain, a reference non-RECAP antenna array is considered, having the same number of feeds and area as the RECAP, but consisting of matched dipoles. Although antennas were placed as far apart as possible for the reference case, some initial experiments were required to find the best placement of feeds for the RECAP to give peak capacity. Having feeds too close to the aperture center or edge reduced the capacity of the RECAP, and a balanced arrangement gave the best performance.

Channel capacity is computed from

$$C = \log_2\left(\det\left[\mathbf{I} + \mathbf{H}\mathbf{R}_{\rm x}\mathbf{H}^H\mathbf{R}_\eta^{-1}\right]\right) \tag{27}$$

and for equal power allocation $\mathbf{R}_{\rm x} = (P_{\rm T}/N_{\rm F})\mathbf{I}$, where $P_{\rm T}$ is the total Tx power, and $N_{\rm F}$ is the number of Tx feeds. Lumping noise covariance into the channel matrix results in

$$\mathbf{H}_\eta = \mathbf{H}\mathbf{R}_\eta^{-1/2} \tag{28}$$

where $\mathbf{R}_\eta^{-1/2}$ is computed using (17). Plugging (28) into (27)

$$C = \log_2\left(\det\left[\mathbf{I} + \frac{P_T}{N_F}\mathbf{H}_\eta\mathbf{H}_\eta^H\right]\right) \tag{29}$$

which can be interpreted as the capacity of an effective channel $\mathbf{H}_\eta$ for i.i.d. noise (unit variance) and transmit power P_T.

A convenient way of enforcing the different power constraints in this study is to first define the average single-input single-output (SISO) gain of a given system as

$$G_{\rm SISO}(\mathbf{H}) = \frac{\|\mathbf{H}\|_{\rm F}^2}{N_{\rm F}N'_{\rm F}} \tag{30}$$

where $\|.\|_{\mathrm{F}}$ is Frobenius norm and N'_{F} is the number of feeds at Rx, which indicates the average power gain provided by channel matrix $\mathbf{H}$ with respect to all active ports. The desired SNR ρ of a system can then be fixed by normalizing that system by its SISO gain according to $\underline{\mathbf{H}}_\eta = G_{\mathrm{SISO}}^{-1/2}(\mathbf{H}_\eta)\mathbf{H}_\eta$ and setting transmit power as $P_T = \rho G_{\mathrm{SISO}}^{-1}(\mathbf{H}_\eta)$, resulting in the equivalent capacity expression

$$C = \log_2\left(\det\left[\mathbf{I} + \frac{\rho}{N_{\mathrm{F}}}\underline{\mathbf{H}}_\eta \underline{\mathbf{H}}_\eta^H\right]\right) \tag{31}$$

where $\underline{\cdot}$ represents the normalized quantity. Below we explain how this normalization can be used to implement power constraints for three realistic cases.

Fixed SNR Constraint (Case 1): The total amount of transmitted/collected power is the same for both the non-RECAP and RECAP structures. This constraint ensures that the RECAP can only increase capacity by improving channel orthogonality or conditioning. For Case 1, channel matrices corresponding to a non-RECAP reference (REF) and the RECAP are normalized as

$$\underline{\mathbf{H}}_{\eta,\mathrm{REF}} = G_{\mathrm{SISO}}^{-1/2}(\mathbf{H}_{\eta,\mathrm{REF}})\mathbf{H}_{\eta,\mathrm{REF}} \tag{32}$$

$$\underline{\mathbf{H}}_\eta = G_{\mathrm{SISO}}^{-1/2}(\mathbf{H}_\eta)\mathbf{H}_\eta. \tag{33}$$

Normalizing each system individually by its own SISO gain forces the RECAP and reference case to both have average SISO SNR ρ when computing capacity with (31).

Max EIRP Constraint (Case 2): Here we constrain the EIRP of the RECAP to be no larger than that of the reference (non-RECAP) system. This is accomplished by setting transmit power P_T such that a prescribed SNR ρ is obtained for the reference system, and this same transmit power is also used for the RECAP system. Maximum EIRP of the RECAP system is then limited to be equal to or lower than that of the reference system by scaling the embedded RECAP radiation patterns according to

$$\underline{\mathbf{e}}_{\mathrm{FT},i}^{\mathrm{mc}}(\phi) = \underbrace{\frac{\max_{\phi,k}\left|\mathbf{e}_{k,\mathrm{REF}}^{\mathrm{mc}}(\phi)\right|}{\max_{\phi}\left|\mathbf{e}_{\mathrm{FT},i}^{\mathrm{mc}}(\phi)\right|}}_{\zeta_i}\mathbf{e}_{\mathrm{FT},i}^{\mathrm{mc}}(\phi) \tag{34}$$

where $\mathbf{e}_{\mathrm{FT},i}^{\mathrm{mc}}(\phi)$ refers to the radiation pattern of the ith feed at Tx, $\mathbf{e}_{i,\mathrm{REF}}^{\mathrm{mc}}(\phi)$ refers to the one corresponding to the ith feed of the reference (non-RECAP) Tx, and $\underline{\mathbf{e}}_{\mathrm{FT},i}^{\mathrm{mc}}(\phi)$ is used in place of $\mathbf{e}_{\mathrm{FT},i}^{\mathrm{mc}}(\phi)$ when computing $\mathbf{S}_{\mathrm{Rx,Tx}}$ in (9) when ζ_i is less than or equal to 1 (i.e. when a RECAP feed provides higher maximum gain than a non-RECAP feed). The non-RECAP and RECAP channels are normalized respectively with (32) and

$$\underline{\mathbf{H}}_\eta = G_{\mathrm{SISO}}^{-1/2}(\mathbf{H}_{\eta,\mathrm{REF}})\mathbf{H}_\eta. \tag{35}$$

Note that although the advantage of transmit beamforming by the RECAP is removed due to the maximum EIRP normalization, both channels are normalized by the SISO gain of the reference system, preserving possible enhanced power collection with *receive* RECAP beamforming.

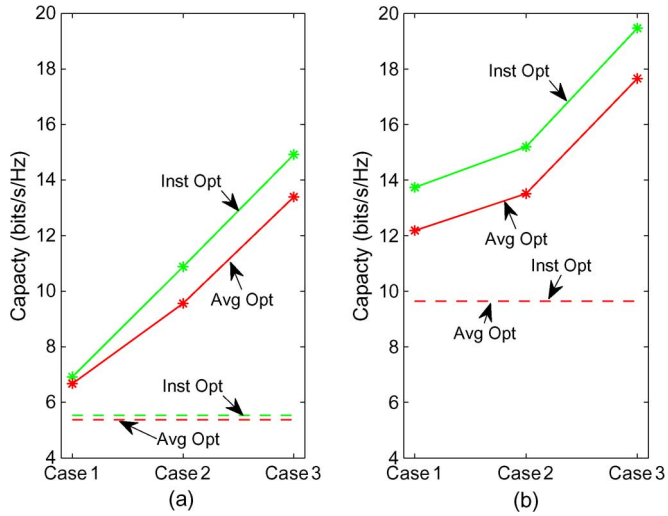

Fig. 4. Instantaneous and average MIMO channel capacity for a simple non-RECAP array (dashed lines) and RECAP (solid lines): (a) 2×2 MIMO with $L = 4$, (b) 4×4 MIMO with $L = 8$.

Average Transmit Power Constraint (Case 3): In this case, only average transmit power is constrained such that a prescribed SNR ρ is obtained for the reference system, and no constraint is placed on directional gain of Tx or Rx antennas. Specifically, channel matrix normalization is done using (32) and (35), allowing the RECAP to obtain a power advantage through both transmit and receive beamforming.

IV. MIMO Capacity Analysis

Since the advantage of RECAP may depend on the number of antennas, we consider both 2×2 and 4×4 MIMO systems. Fig. 1 shows the top view of transmit/receive antennas for the RECAP and non-RECAP structures for the analyzed 2×2 and 4×4 MIMO systems. Results are for the uniform path-based model and reference SNR $\rho = 10$ dB, unless otherwise noted.

A. Single User MIMO Capacity

Channel capacity for single user communication is computed using (31) where $\underline{\mathbf{H}}_\eta$ is computed using the cases in Section III.

1) 2 × 2 MIMO System: Fig. 4(a) plots the capacity for the RECAP and non-RECAP structures for average and instantaneous optimization. Note that capacity for the non-RECAP does not change with constraint type, since the reference has constant SNR, and the slight difference with respect to optimization type is due to different Monte Carlo realizations. For fixed SNR (Case 1), RECAP capacity is only marginally better than that of the non-RECAP, indicating that two channels of sufficient quality are obtained without reconfigurability, and the RECAP cannot significantly improve this.

The main advantage of RECAP is power, with significant improvements seen when moving to the EIRP constraint (Case 2) and the transmit power constraint (Case 3). It is also apparent that average optimization is only slightly worse than instantaneous optimization, which is reasonable for power enhancement, since multi-path *directions* are mainly important, not the *phases* of signals sent in those directions.

2) 4 × 4 MIMO System: Fig. 4(b) shows that RECAP performance is more flat with respect to the constraint type for the 4 × 4 MIMO system, suggesting that power advantage is less important and more opportunity for improving channel conditioning exists. Also a more significant gap is seen between average and instantaneous optimization, indicating not only mutli-path directions but also phases are important to attain peak capacity. Finally it is interesting that the transmit power constraint for the 2 × 2 RECAP system gives almost the same performance as the 4 × 4 system with the EIRP constraint.

B. Single User MIMO Under Interference Constraint

Most practical systems for personal wireless communications are interference limited, and we therefore study the effect of interference on single-link capacity in detail. In order to model the effect of interference, we extend $\mathbf{R}'_\eta$ to be the covariance matrix of noise and interference, or

$$\mathbf{R}'_\eta = \mathbf{R}_\eta + \widehat{\mathbf{H}}\widehat{\mathbf{H}}^H \frac{\widehat{P}_\mathrm{T}}{\widehat{N}_\mathrm{F}} \tag{36}$$

where $\widehat{\mathbf{H}}$ represents the channel matrix between the interferer and receiving antennas, other $\widehat{\cdot}$ quantities are for interferer, analogous to those at Tx, and we assume $\widehat{N}_\mathrm{F} = N_\mathrm{F}$. Plugging (36) into (27) and simplifying yields

$$C = \log_2\left(\det\left[\mathbf{I} + \frac{\rho}{N_\mathrm{F}}\left(\mathbf{I} + \frac{\widehat{\rho}}{\widehat{N}_\mathrm{F}}\underline{\widehat{\mathbf{H}}}_\eta\underline{\widehat{\mathbf{H}}}_\eta^H\right)^{-1}\underline{\mathbf{H}}_\eta\underline{\mathbf{H}}_\eta^H\right]\right) \tag{37}$$

where $\widehat{\rho} = G_\mathrm{SISO}(\widehat{\mathbf{H}}_\eta)\widehat{P}_T$ is interference-to-noise ratio. Since $\widehat{\rho}$ depends on proximity of the interferer, values of $\widehat{\rho}$ between 0 to 20 dB are considered. We assume that the interfering node employs a non-RECAP structure and $\widehat{\mathbf{S}}_{\mathrm{Rx,Tx}}$ is computed as

$$\widehat{\mathbf{S}}_{\mathrm{Rx,Tx}} = \sum_{k=1}^{\widehat{K}}\sum_{\ell=1}^{\widehat{L}_k}\left[\mathbf{E}_\mathrm{FT}^{\mathrm{mc}'}\left(\widehat{\theta}'_{k\ell}, \widehat{\phi}'_{k\ell}\right)\right]^T \widehat{\alpha}_{k\ell}e^{-j\omega\widehat{\tau}_{k\ell}}\widehat{\mathbf{E}}_\mathrm{FT}^{\mathrm{mc}}(\widehat{\theta}_{k\ell}, \widehat{\phi}_{k\ell}). \tag{38}$$

1) 2 × 2 MIMO System: Fig. 5(a) plots the capacity of a 2 × 2 system with $L = 4$ multi-path for both non-RECAP and RECAP. The case for $\widehat{\rho} = 0$ dB, is similar to no interference. As $\widehat{\rho}$ increases, non-RECAP capacity steadily drops towards zero, since for interference with rank $\widehat{N}_\mathrm{F} = N_\mathrm{F}$, it is not possible for the non-RECAP to null the effect. Although capacity for both the non-RECAP and RECAP is falling with increasing $\widehat{\rho}$, closer inspection reveals that the capacity gain of using the RECAP over the non-RECAP actually increases with increasing $\widehat{\rho}$. Performance degradation is much smaller for the RECAP since REs can be used to null interference, suggesting the possibility of aggressive spectral reuse.

2) 4 × 4 MIMO System: The results for varying $\widehat{\rho}$ are shown in Fig. 6(a) for $L = 8$. The overall effect is same as that of 2 × 2 system, but the curves are flatter with respect to the power constraint, indicating that power advantage is less important for more feeds for fixed interference as well. However, improvement relative to the non-RECAP is still very significant, especially for severe interference.

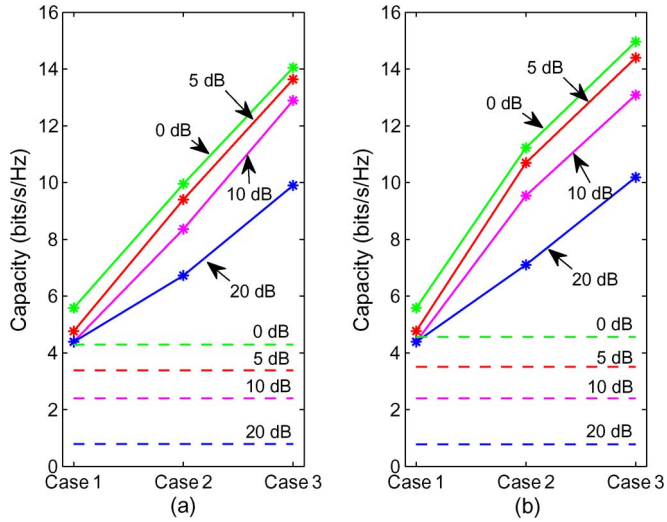

Fig. 5. Channel capacity for single user 2 × 2 MIMO with fixed interference for a simple non-RECAP array (dashed lines) and RECAP (solid lines): (a) uniform multi-path $L = 4$, (b) SVA model.

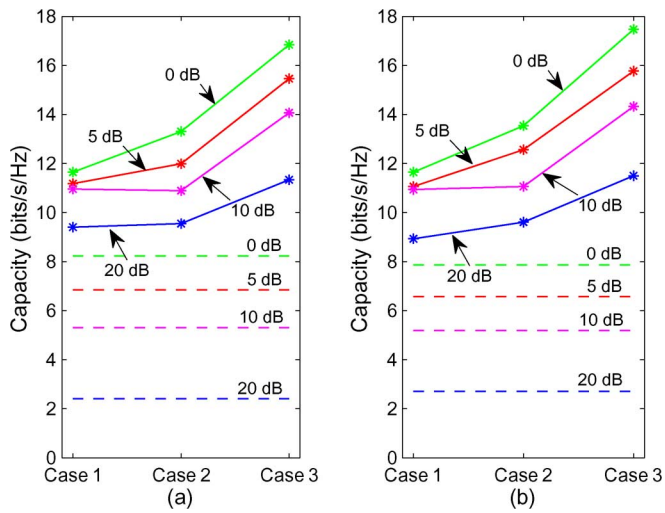

Fig. 6. Channel capacity for single user 4 × 4 MIMO with fixed interference for a simple non-RECAP array (dashed lines) and RECAP (solid lines): (a) uniform multi-path with $L = 8$, (b) SVA model.

C. Multi-User MIMO

Building on the idea of employing aggressive spectral reuse, we next consider a true multi-user scenario where users optimize their RECAPs to maximize sum capacity. This is different from the case of fixed interference, since the role of the transmit RECAP becomes more important to reduce interference to the other user. Although for fixed interference, the user does not have control over interference, he also does not care about how much interference he causes. For the multi-user case, interference can be controlled but users also impact each other. Capacity degradation due to interference depends on proximity, and $\widehat{\rho}$ between 0 and 20 dB is again considered.

Two links are considered, where each receiving user experiences interference from the transmitter of the other link and a joint optimization is done in order to maximize the sum capacity

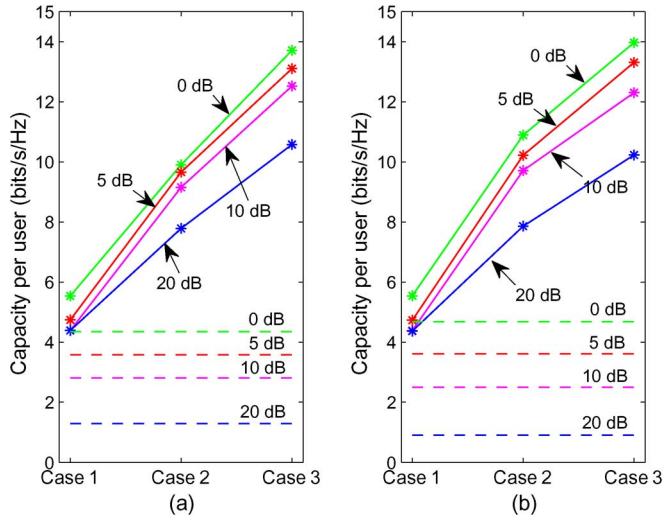

Fig. 7. Channel capacity for two-user 2 × 2 MIMO for a simple non-RECAP array (dashed lines) and RECAP (solid lines): (a) uniform mutli-path with $L = 4$, (b) SVA model.

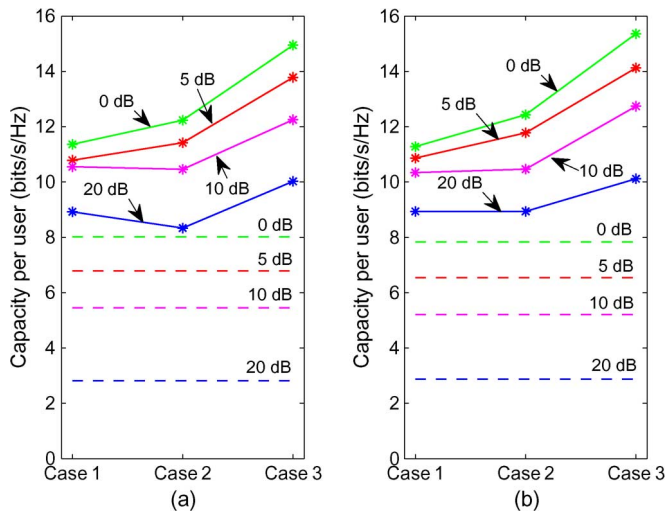

Fig. 8. Channel capacity for two-user 4 × 4 MIMO for a simple non-RECAP array (dashed lines) and RECAP (solid lines): (a) uniform mutli-path with $L = 8$, (b) SVA model.

of both links. Individual capacity of each link is calculated using (37), except now in (38), the Tx RECAP patterns of the other link are employed instead of $\widehat{\mathbf{E}}_{\mathrm{FT}}^{\mathrm{mc}}(\widehat{\theta}_{k\ell}, \widehat{\phi}_{k\ell})$ for a non-RECAP. Fig. 7(a) shows MIMO channel capacity per user for the 2 × 2 multi-user system with increasing $\widehat{\rho}$, exhibiting similar RECAP capacity gain as the fixed interference case. The relative gain in moving from Case 1 to Case 2 is higher for multi-user compared the single user case with fixed interference, likely due to the fact that Tx RECAPs can now be controlled to avoid interference.

Fig. 8(a) shows the results for the 4 × 4 MIMO system. By increasing $\widehat{\rho}$, the improvement with respect to constraint type becomes even flatter than the 4 × 4 case for fixed interference. Surprisingly, RECAP capacity per user is now lower than that for fixed interference, indicating that jointly suppressing incoming interference and avoiding outgoing interference becomes more difficult for more active feeds.

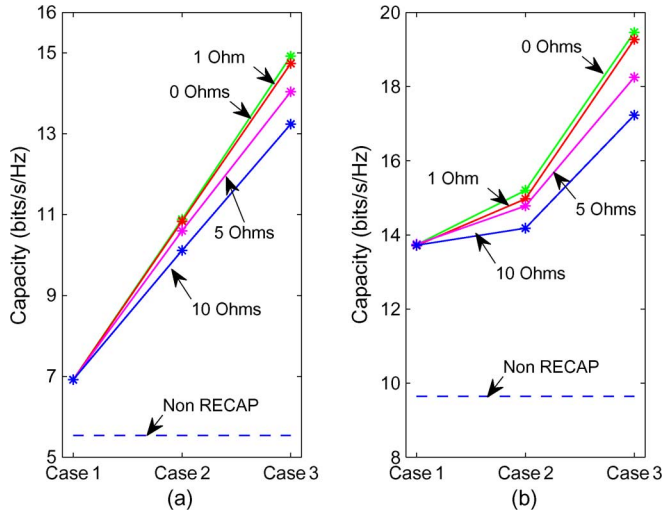

Fig. 9. Effect of losses for a simple non-RECAP array (dashed lines) and RECAP (solid lines): (a) 2 × 2 MIMO with uniform multi-path and $L = 4$, (b) 4 × 4 MIMO with uniform multi-path and $L = 8$.

D. SVA Propagation Model

The simple path-based model is convenient, but possibly over-simplistic to represent true propagation scenarios, and hence we also consider the Saleh Valenzuela Angular (SVA) model [18]. The parameters of the model are assumed to be $T_C = 34$ ns, $T_R = 29$ ns, $1/\Lambda = 17$ ns, $1/\lambda = 5$ ns and $\sigma = 26°$, taken from [18]. The model makes use of a threshold value after which it stops looking for multi-path, which we have assumed to be −10 dB, generating 50 multi-path on average.

Results for SVA channel simulations have been plotted next to the respective plots for the simple path-based model in Figs. 5–8. There is not a dramatic impact compared to the simple channel model. For the non-RECAP case, capacity is slightly more degraded in some results with increasing $\widehat{\rho}$ due to more paths. For the RECAP case the curve trends are similar, but curves are shifted up slightly in some results showing that RECAP is more advantageous with increased multi-path. However, in general changes are only marginal.

E. Effects of Losses and Bandwidth on Channel Capacity

Bandwidth limitations and RE loss are important considerations in practical RECAP structures, and in this section we study these two effects. First we consider loss by including a series resistance with each RE ranging from 0–10 Ω. Fig. 9(a) shows the results corresponding to the 2 × 2 single user system without any interference. There is no impact of loss for Case 1 since power differences are removed. Moving to Cases 2 and 3, the impact of loss becomes increasingly prominent, resulting from reduced gain of the RECAP, which decreases the channel capacity. More performance loss is observed for the 4 × 4 MIMO system as shown in Fig. 9(b).

Another important aspect is finite bandwidth, and in order to study its effect a two sided bandwidth of 20 MHz is assumed at a center frequency of 3 GHz. Capacity is computed as the average capacity at the center frequency and two band edges for a single fixed RECAP structure. Channels are normalized as

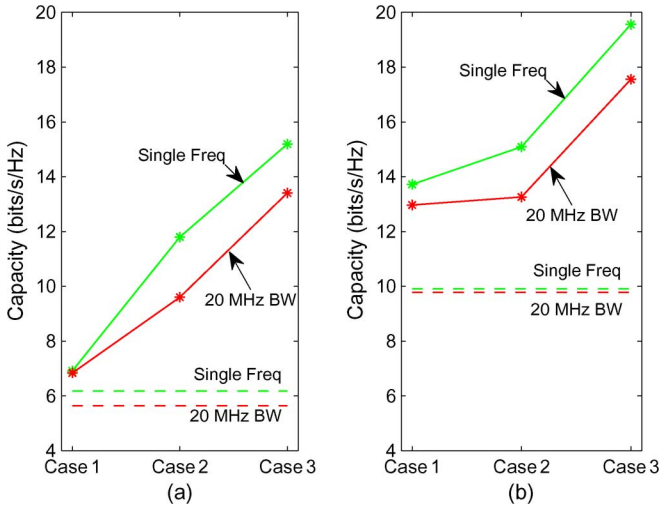

Fig. 10. RECAP capacity for 20 MHz bandwidth and the SVA model for a simple non-RECAP array (dashed lines) and RECAP (solid lines): (a) 2×2, (b) 4×4.

before, except now the largest (worst case) normalization factor of the three frequencies is used.

Fig. 10(a) indicates that finite bandwidth results in a small capacity reduction for the 2×2 non-RECAP. Although RECAP performance is minimally impacted in Case 1, for Cases 2 and 3 some reduction is seen, comparable to the difference of average versus instantaneous optimization. Results for the 4×4 system in Fig. 10(b) are similar with a slightly larger gap between single frequency and finite bandwidth curves.

V. Conclusion

This work has analyzed MIMO capacity improvements possible with a simple RECAP structure for different scenarios and system power constraints. The results indicate that very large gains relative to fixed antenna MIMO systems are possible, especially for interference-limited and multi-user environments, suggesting that RECAPs may enable aggressive spectral reuse. Consideration of finite bandwidth and losses has indicated that RECAPs can also provide most of this capacity improvement even with these practical impairments.

References

[1] E. Telatar, "Capacity of multi-antenna Gaussian channels," *Eur. Trans. Telecommun.*, vol. 10, no. 6, pp. 585–595, 1999.

[2] R. S. Blum, "MIMO capacity with interference," *IEEE J. Sel. Areas Commun.*, vol. 21, no. 5, pp. 793–801, 2003.

[3] M. A. Jensen and J. W. Wallace, "Capacity of the continuous-space electromagnetic channel," *IEEE Trans. Antennas Propag.*, vol. 56, no. 2, pp. 524–531, 2008.

[4] A. Alexiou and M. Haardt, "Smart antenna technologies for future wireless systems: Trends and challenges," *IEEE Commun. Mag.*, vol. 42, no. 9, pp. 90–97, 2004.

[5] L. N. Pringle, P. H. Harms, S. P. Blalock, G. N. Kiesel, E. J. Kuster, P. G. Friederich, R. J. Prado, J. M. Morris, and G. S. Smith, "A reconfigurable aperture antenna based on switched links between electrically small metallic patches," *IEEE Trans. Antennas Propag.*, vol. 52, no. 6, pp. 1434–1445, 2004.

[6] J. H. Schaffner, R. Y. Loo, D. F. Sievenpiper, F. A. Dolezal, G. L. Tangonan, J. S. Colburn, J. J. Lynch, J. J. Lee, S. W. Livingston, R. J. Broas, and M. Wu, "Reconfigurable aperture antennas using RF MEMS switches for multi-octave tunability and beam steering," in *Proc. IEEE Antennas Propag. Society Int. Symp*, 2000, vol. 1, pp. 321–324.

[7] A. F. Molisch, M. Z. Win, Y.-S. Choi, and J. H. Winters, "Capacity of MIMO systems with antenna selection," *IEEE Trans. Wireless Commun.*, vol. 4, no. 4, pp. 1759–1772, 2005.

[8] M. D. Migliore, D. Pinchera, and F. Schettino, "Improving channel capacity using adaptive MIMO antennas," *IEEE Trans. Antennas Propag.*, vol. 54, no. 11, pp. 3481–3489, 2006.

[9] C. Waldschmidt and W. Wiesbeck, "Compact wide-band multimode antennas for MIMO and diversity," *IEEE Trans. Antennas Propag.*, vol. 52, no. 8, pp. 1963–1969, 2004.

[10] B. A. Cetiner, E. Akay, E. Sengul, and E. Ayanoglu, "A MIMO system with multifunctional reconfigurable antennas," *IEEE Antennas Wireless Propag. Lett.*, vol. 5, no. 1, pp. 463–466, 2006.

[11] D. Piazza, N. J. Kirsch, A. Forenza, R. W. Heath, and K. R. Dandekar, "Design and evaluation of a reconfigurable antenna array for MIMO systems," *IEEE Trans. Antennas Propag.*, vol. 56, no. 3, pp. 869–881, 2008.

[12] A. Grau, H. Jafarkhani, and F. De Flaviis, "A reconfigurable multiple-input multiple-output communication system," *IEEE Trans. Wireless Commun.*, vol. 7, no. 5, pp. 1719–1733, 2008.

[13] F. Fazel, A. Grau, H. Jafarkhani, and F. Flaviis, "Space-time-state block coded MIMO communication systems using reconfigurable antennas," *IEEE Trans. Wireless Commun.*, vol. 8, no. 12, pp. 6019–6029, 2009.

[14] M. L. Morris and M. A. Jensen, "Network model for MIMO systems with coupled antennas and noisy amplifiers," *IEEE Trans. Antennas Propag.*, vol. 53, no. 1, pp. 545–552, 2005.

[15] R. Mehmood and J. W. Wallace, "Diminishing returns with increasing complexity in reconfigurable aperture antennas," *IEEE Antennas Wireless Propag. Lett.*, vol. 9, pp. 299–302, 2010.

[16] G. Gonzalez, *Microwave Transistor Amplifiers*. Englewood Cliffs, NJ: Prentice-Hall, 1997.

[17] MAXIM, July 2004, "Low-Noise Amplifier (LNA) Matching Techniques for Optimizing Noise Figures," MAXIM [Online]. Available: http://pdfserv.maxim-ic.com/en/an/AN3169.pdf

[18] Q. H. Spencer, B. D. Jeffs, M. A. Jensen, and A. L. Swindlehurst, "Modeling the statistical time and angle of arrival characteristics of an indoor multipath channel," *IEEE J. Sel. Areas Commun.*, vol. 18, no. 3, pp. 347–360, 2000.

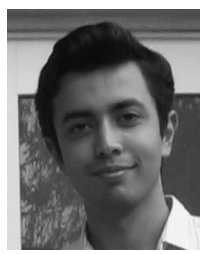

Rashid Mehmood (S'05) received the B.Sc. degree (*cum laude*) in communication systems engineering from the Institute of Space Technology (IST), Pakistan, in 2007 and the M.Sc. degree in electrical engineering from Jacobs University Bremen (JUB), Bremen, Germany, in 2010.

From 2007 to 2008, he worked as a Research Associate at IST and supervised various undergraduate laboratories. From 2008 to 2010, he worked as a Research Assistant in several laboratories at JUB and external companies. His current research interests include reconfigurable aperture antennas, antenna optimization and wireless and optical communications.

Mr. Mehmood was a recipient of the 2009 IEEE AP-S Undergraduate Research Award.

Jon W. Wallace (S'99–M'03) received the B.S. (*summa cum laude*) and Ph.D. degrees in electrical engineering from Brigham Young University (BYU), Provo, UT, in 1997 and 2002, respectively.

He received the National Science Foundation Graduate Fellowship in 1998 and worked as a Graduate Research Assistant at BYU until 2002. From 2002 to 2003, he was with the Mobile Communications Group, Vienna University of Technology, Vienna, Austria. From 2003 to 2006, he was a Research Associate with the BYU Wireless Communications Laboratory. Since 2006, he has been an Assistant Professor of electrical engineering at Jacobs University, Bremen, Germany. His current research interests include MIMO wireless systems, physical-layer security, cognitive radio and UWB systems.

Dr. Wallace is serving as an Associate Editor of the IEEE Transactions on Antennas and Propagation and is a Co-Guest Editor of the Special Issue on Multiple-Input Multiple-Output (MIMO) Technology.